Chinese Journal of Natural Medicines

***Dendrobium officinale* inhibits colorectal cancer progression by induction of glutathione peroxidase 4–mediated ferroptosis**

Ruidi Jiang, Xuanjing Tan, Guiyu Zhang, Haipeng Chen, Hong Yu, Yuting Zheng, Muyan Kong, Keyao Shan, Jiyao Liu, Rong Zhang, Zhongqiu Liu, Jinjun Wu

Citation: Ruidi Jiang, Xuanjing Tan, Guiyu Zhang, Haipeng Chen, Hong Yu, Yuting Zheng, Muyan Kong, Keyao Shan, Jiyao Liu, Rong Zhang, Zhongqiu Liu, Jinjun Wu, *Dendrobium officinale* inhibits colorectal cancer progression by induction of glutathione peroxidase 4–mediated ferroptosis, Chinese Journal of Natural Medicines, 2026, 24(3), 338–348. doi: 10.1016/S1875–5364(26)61108–9.

View online: https://doi.org/10.1016/S1875–5364(26)61108–9

Chinese Journal of Natural Medicines 24 (2026) 338-348

Contents lists available at ScienceDirect

Chinese Journal of Natural Medicines

journal homepage: www.cjnmcpu.com/

Original article

Dendrobium officinale inhibits colorectal cancer progression by induction of glutathione peroxidase 4-mediated ferroptosis

Ruidi Jiang[a,Δ], Xuanjing Tan[a,Δ], Guiyu Zhang[a,b,Δ], Haipeng Chen[a], Hong Yu[a], Yuting Zheng[a], Muyan Kong[a,b], Keyao Shan[a], Jiyao Liu[a], Rong Zhang[a], Zhongqiu Liu[a,*], Jinjun Wu[a,*]

[a] *State Key Laboratory of Traditional Chinese Medicine Syndrome, Guangdong Provincial Key Laboratory of Translational Cancer Research of Chinese Medicines, Joint International Research Laboratory of Translational Cancer Research of Chinese Medicines, International Institute for Translational Chinese Medicine, School of Pharmaceutical Sciences, Guangzhou University of Chinese Medicine, Guangzhou 510006, China*

[b] *The Seventh Affiliated Hospital of Guangzhou University of Chinese Medicine, Shenzhen 518000, China*

ARTICLE INFO

Article history:
Received 19 February 2025
Revised 8 May 2025
Accepted 13 May 2025
Available online 20 March 2026

Keywords:
Colorectal cancer
Dendrobium officinale
Ferroptosis
Glutathione peroxidase 4
Lipid peroxidation

ABSTRACT

Colorectal cancer (CRC), one of the leading causes of cancer-related mortality globally, urgently requires complementary and alternative therapies. Ferroptosis, an iron-dependent form of regulated cell death driven by lipid peroxidation, has emerged as a promising anticancer strategy. *Dendrobium officinale* (*D. officinale*), a renowned traditional Chinese medicinal herb, is widely used in several Asian countries for its nutritional and therapeutic benefits. Although *D. officinale* has demonstrated anti-tumor effects, the molecular mechanisms underlying its action against CRC remain incompletely characterized. This study aimed to elucidate the role of *D. officinale* in suppressing CRC through the induction of ferroptosis and its regulatory effects on glutathione peroxidase 4 (GPX4), a key suppressor of ferroptosis. *In vitro* assays were conducted using HCT116 and SW480 CRC cell lines, and *in vivo* efficacy was evaluated in BALB/c nude mice bearing CRC xenografts. D. officinale significantly reduced CRC cell viability and proliferation *in vitro* and suppressed tumor growth *in vivo*. Induction of ferroptosis was evidenced by elevated levels of Fe^{2+}, malondialdehyde (MDA), and lipid peroxidation, along with a depleted glutathione/oxidized glutathione disulfide (GSH/GSSG) ratio. Notably, these effects were reversed by ferroptosis inhibitors, including ferrostatin-1 (Fer-1) and deferoxamine. Consistently, *D. officinale* markedly downregulated GPX4 expression. Overexpression of GPX4 rescued *D. officinale*-induced ferroptosis, whereas GPX4 silencing exacerbated this effect. *D. officinale* suppresses CRC by triggering GPX4-dependent ferroptosis, providing a novel, naturally derived therapeutic approach. These findings bridge traditional medicine and modern oncology, establishing a foundation for developing targeted CRC treatments.

1. Introduction

Colorectal cancer (CRC) ranks third in global cancer incidence, with over 1.9 million new cases and approximately 900,000 deaths annually, highlighting the urgent need for innovative therapeutic strategies [1]. Despite advances in conventional treatments such as surgery, chemotherapy, and immunotherapy, significant limitations persist, including drug resistance [2], off-target toxicity [3], and high recurrence rates [4]. These challenges underscore the necessity for alternative approaches that selectively target malignant cells while preserving healthy tissues.

Ferroptosis, a regulated form of cell death driven by iron-dependent lipid peroxidation, has emerged as a promising therapeutic pathway [5]. Unlike apoptosis or necrosis, ferroptosis is characterized by the accumulation of reactive oxygen species (ROS) and depletion of glutathione (GSH), culminating in irreversible membrane damage [6]. Central to this process is glutathione peroxidase 4 (GPX4), an enzyme that utilizes GSH to detoxify lipid hydroperoxides [7]. Inhibition of GPX4 disrupts redox homeostasis, thereby sensitizing cancer cells to ferroptotic cell death. Preclinical studies have demonstrated the efficacy of GPX4-targeting agents in CRC models; however, clinical translation remains limited by systemic toxicity and synthetic complexity [8].

Traditional Chinese medicine (TCM) represents a rich source of natural compounds with multitarget pharmacological activities and favorable safety profiles [9]. *Dendrobium officinale* (*D. officinale*), a key epiphytic orchid species, is widely recognized for its dual status as both food and medicine due to its homologous properties [10]. It has been traditionally employed across various Asian countries for its nutritional value and diverse therapeutic effects [11]. The bioactivity of *D. officinale* is attributed to its abundance of active constituents, including polysaccharides, flavonoids, and alkaloids [12]. Pharmacological evidence indicates that *D. officinale* exerts multiple beneficial effects, such as lipid-lowering and immunomodulatory actions [13, 14], restoration of intestinal barrier integrity [15], and attenuation of oxidative stress and

* Corresponding author.
E-mail addresses: liuzq@gzucm.edu.cn (Z. Liu); wujinjun@gzucm.edu.cn (J. Wu)
Δ These authors contributed equally to this work.

https://doi.org/10.1016/S1875-5364(26)61108-9

neuroinflammation [16]. In traditional practice, it is valued for nourishing Yin, clearing heat, promoting fluid production, and supporting gastric health [17, 18]. Additionally, it is applied in liver disease management, where it contributes to hepatic nourishment and functional improvement [19]. Notably, *D. officinale* extracts suppress CRC cell proliferation and metastasis, although the underlying molecular mechanisms remain poorly understood [20]. Given its documented influence on oxidative stress and lipid metabolism, we hypothesized that *D. officinale* may induce ferroptosis in CRC cells *via* modulation of GPX4 expression.

This study integrates *in vitro* and *in vivo* methodologies to investigate the role of *D. officinale* in ferroptosis-mediated suppression of CRC. First, we assessed the inhibitory effects of *D. officinale* on human CRC cell viability and proliferation using *in vitro* assays. Next, a xenograft CRC model was established in BALB/c nude mice to evaluate tumor-suppressive effects *in vivo*. We then examined the capacity of *D. officinale* to trigger ferroptosis in CRC cells. Furthermore, we analyzed how *D. officinale* regulates GPX4 expression at the molecular level. Finally, we validated the functional involvement of GPX4 in *D. officinale*-induced ferroptosis through gain-of-function and loss-of-function experiments involving GPX4 overexpression and silencing. These findings are expected to deepen understanding of the molecular basis underlying the anti-cancer activity of *D. officinale* in CRC and provide robust preclinical evidence supporting its potential future application in CRC therapy.

2. Materials and methods

2.1. Chemicals and reagents

The GSH assay kit was obtained from Beyotime (Shanghai, China), while the malondialdehyde (MDA) assay kit was sourced from Jiancheng Bioengineering Institute (Nanjing, China). Oxaliplatin (Oxa, purity ≥ 98.0%), ferrostatin-1 (Fer-1, purity ≥ 99.59%), and deferoxamine mesylate (DFO, purity ≥ 99.86%) were purchased from MedChemExpress (Monmouth Junction, NJ, USA). C11-BODIPY 581/591 fluorescent dye was acquired from Thermo Fisher Scientific (Waltham, MA, USA). GPX4 and β-actin primary antibodies were obtained from Abmart Shanghai Co., Ltd. (Shanghai, China). All other chemicals were of analytical grade or higher.

2.2. Cell lines

HCT116 and SW480 human colorectal cancer (CRC) cell lines, as well as NCM460 normal human colonic epithelial cells, were obtained from the American Type Culture Collection (ATCC, Manassas, VA, USA). Cells were cultured in Dulbecco's modified Eagle medium (DMEM, Gibco, USA) or RPMI-1640 (Gibco) supplemented with 10% fetal bovine serum (FBS, Gibco) and 1% penicillin/streptomycin (Invitrogen, USA). All cells were maintained in a humidified incubator at 37 °C with 5% CO_2, and the culture medium was replaced every 48 h.

2.3. Preparation of *D. officinale* extract and LC-MS/MS analysis

The *D. officinale* specimen (HX21L01.209) was provided by Guangdong Hexiang Pharmaceutical Co., Ltd. and authenticated by taxonomic experts. A voucher specimen was deposited at the Laboratory of the International Institute for Translational Chinese Medicine, Guangzhou University of Chinese Medicine (Guangzhou, China). Detailed procedures for preparing the *D. officinale* extract and conducting LC-MS/MS analysis are described in the Supplementary Materials and Methods [21]. Chemical profiling results are presented in Supplementary Fig. 1.

2.4. Cell viability assay

Cells (5×10^3 cells/well) were seeded into 96-well plates (Corning, USA) and allowed to adhere overnight. Subsequently, cells were treated with *D. officinale* (5–40 mg·mL^{-1}) or Oxa (100 μmol·L^{-1}) for 24 h. After treatment, methyl thiazolyl tetrazolium (MTT) reagent (0.5 mg·mL^{-1}, Sigma-Aldrich) was added, followed by 4 h of incubation. Formazan crystals were dissolved in 100 μL DMSO per well, and absorbance was measured at 570 nm using a microplate reader (Molecular Devices, USA), with background correction at 690 nm.

2.5. Cell colony formation assay

Cells were seeded at a density of 500 cells per well in 6-well plates (Corning, USA) and treated with *D. officinale* at 10, 15, and 20 mg·mL^{-1} (HCT116) or 5, 10, and 15 mg·mL^{-1} (SW480), or with Oxa (100 μmol·L^{-1}) for 24 h. Following treatment, cells were gently washed with phosphate-buffered saline (PBS) and cultured in fresh medium for 10 d. Colonies were fixed with 4% paraformaldehyde (PFA, Beyotime, China) for 15 min, stained with 0.1% crystal violet solution (Beyotime) for 30 min, rinsed with distilled water, and air-dried. Colonies containing more than 50 cells were counted manually under a light microscope.

2.6. EdU proliferation assay

The click-iT EdU imaging kit was used to perform the EdU proliferation assay. Cells (8×10^3/well) were seeded in 96-well plates and treated with *D. officinale* at 10, 15, and 20 mg·mL^{-1} (HCT116) or 5, 10, and 15 mg·mL^{-1} (SW480), or with Oxa (100 μmol·L^{-1}) for 24 h. After treatment, cells were incubated with 10 μmol·L^{-1} EdU for 2 h, fixed with 4% PFA, permeabilized with 0.3% Triton X-100, and labeled with Alexa Fluor 488 azide. Nuclei were counterstained with Hoechst 33342 (1 μg·mL^{-1}). Fluorescence images were captured using a fluorescence microscope (Germany), and proliferation rates were calculated as the percentage of EdU-positive nuclei.

2.7. Measurement of intracellular Fe^{2+} levels

Intracellular labile Fe^{2+} levels were measured using the fluorescent probe FeRhoNox-1. HCT116 cells were treated with *D. officinale* at 10, 15, and 20 mg·mL^{-1}, alone or in combination with DFO (100 μmol·L^{-1}) or Fer-1 (1 μmol·L^{-1}). SW480 cells were treated with *D. officinale* at 5, 10, and 15 mg·mL^{-1}, alone or in combination with DFO (100 μmol·L^{-1}) or Fer-1 (1 μmol·L^{-1}). After 24 h, cells were incubated with 5 μmol·L^{-1} FeRhoNox-1 in serum-free medium for 30 min at 37 °C in the dark. Cells were then washed three times with PBS, and fluorescence signals were visualized using a confocal microscope (Leica, Germany).

2.8. Measurement of lipid peroxidation

Lipid peroxidation was assessed using C11-BODIPY 581/591. HCT116 cells were exposed to *D. officinale* at 10, 15, and 20 mg·mL^{-1}, alone or combined with DFO (100 μmol·L^{-1}) or Fer-1 (1 μmol·L^{-1}). SW480 cells were treated with *D. officinale* at 5, 10, and 15 mg·mL^{-1}, alone or in combination with DFO (100 μmol·L^{-1}) or Fer-1 (1 μmol·L^{-1}). After 24 h, cells were incubated with 5 μmol·L^{-1} C11-BODIPY for 30 min at 37 °C, protected from light, washed with PBS, and analyzed immediately. For flow cytometry, cells were trypsinized, resuspended in PBS, and analyzed using a BD FACSAria III (BD Biosciences, USA). FlowJo v10.8 was used for data processing. For microscopy, cells were imaged using a Leica SP8 confocal system (Leica, Germany).

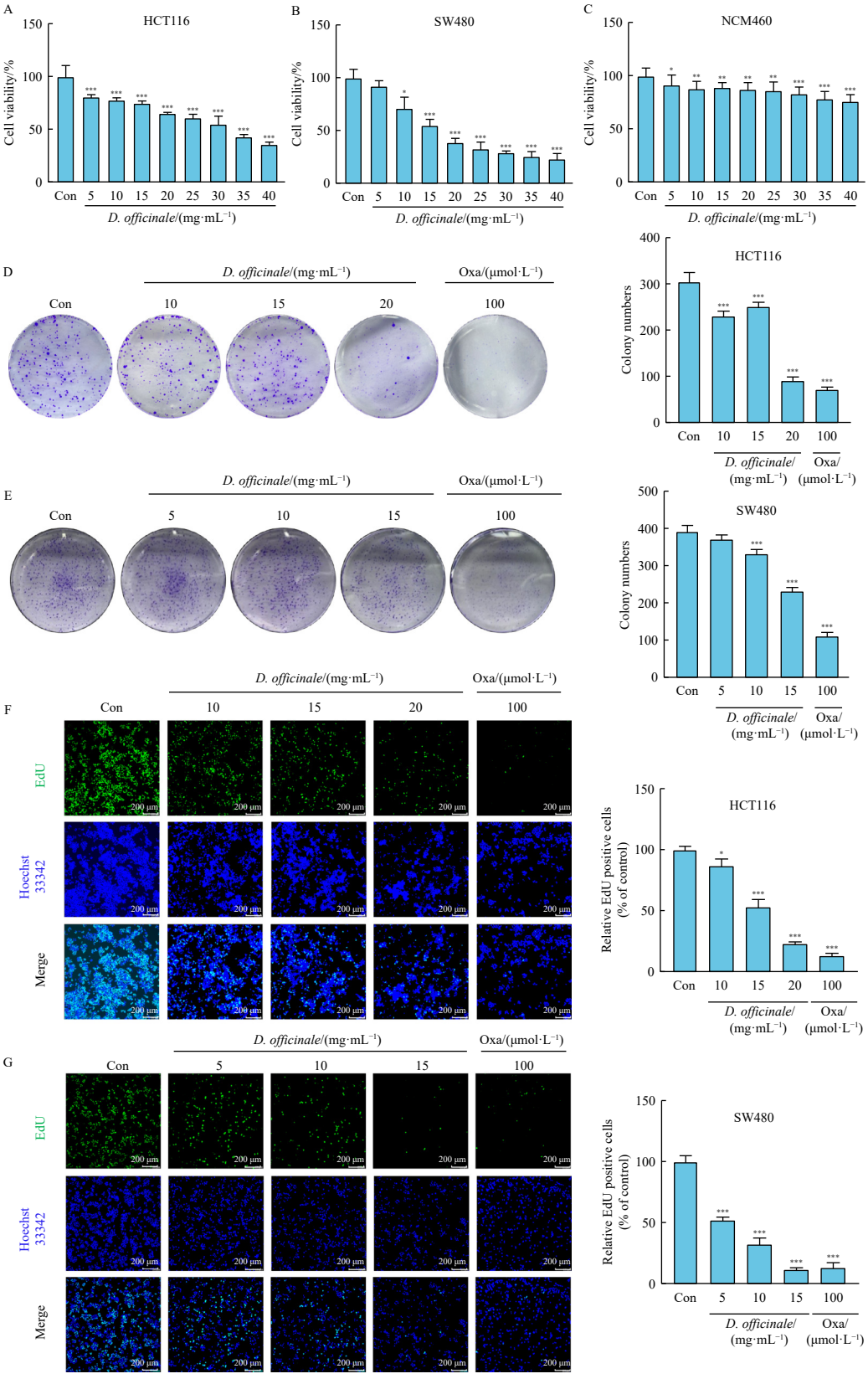

Fig. 1 *D. officinale* inhibits CRC cell viability and proliferation *in vitro*. The impact of *D. officinale* on the viability of HCT116 (A), SW480 (B), and NCM460 (C) cells was assessed following exposure to concentrations between 5 and 40 mg·mL^{-1} for 24 h. The colony formation ability of HCT116 cells was examined after treatment with *D. officinale* at 10, 15, and 20 mg·mL^{-1} (D). For SW480 cells, colony formation was evaluated following exposure to *D. officinale* at concentrations of 5, 10, and 15 mg·mL^{-1} for 24 h (E). The effect of *D. officinale* on the proliferation of HCT116 (F) and SW480 (G) cells was investigated after a 24-h treatment period. Oxa (100 μmol·L^{-1} for 24 h) was used as a positive control for suppression of CRC cells. Data are expressed as mean ± SD (n = 3). $^{*}P < 0.05$, $^{**}P < 0.01$, and $^{***}P < 0.001$ *vs* untreated controls.

2.9. Measurement of MDA levels and glutathione/oxidized glutathione disulfide (GSH/GSSG) ratios

MDA levels and GSH/GSSG ratios were determined using commercial assay kits (Beyotime). HCT116 cells were treated with *D. officinale* at 10, 15, and 20 mg·mL^{-1}, with the highest concentration also tested in combination with DFO (100 μmol·L^{-1}) or Fer-1 (1 μmol·L^{-1}). Similarly, SW480 cells were exposed to *D. offi-*

cinale at 5, 10, and 15 mg·mL^{-1}, with the highest dose combined with DFO or Fer-1. After 24 h of treatment, MDA levels and GSH/GSSG ratios were quantified according to the manufacturer's instructions.

2.10. Mitochondrial membrane potential (ΔΨm)

The mitochondrial membrane potential (ΔΨm) was evaluated using JC-1 dye (10 μg·mL^{-1}, Sigma-Aldrich). HCT116 cells were treated with *D. officinale* at 10, 15, and 20 mg·mL^{-1}, alone or in combination with DFO (100 μmol·L^{-1}) or Fer-1 (1 μmol·L^{-1}). SW480 cells received corresponding treatments at 5, 10, and 15 mg·mL^{-1}, with or without inhibitors. After 24 h, cells were stained with JC-1 dye for 30 min following the manufacturer's protocol. Fluorescence intensities of JC-1 monomers (green emission at 529 nm) and aggregates (red emission at 590 nm) were measured using a confocal fluorescence microscope (Leica, Germany).

2.11. Western blot analysis

Total protein was extracted from cells and colon tissues using RIPA buffer (Beyotime) supplemented with protease inhibitors. Lysates (30 μg/lane) were separated by 12% SDS-PAGE and transferred onto PVDF membranes (Millipore, USA). Membranes were blocked with 5% non-fat milk and incubated overnight at 4 °C with primary antibodies against GPX4 (1∶1000, Abmart, China) and *β*-actin (1∶3000, Abmart, China). After washing, HRP-conjugated secondary antibodies were applied for 1 h. Immunoreactive bands were visualized using ECL reagent (Bio-Rad, USA), and band intensities were quantified using ImageJ software.

2.12. Immunofluorescence staining

HCT116 cells were treated with *D. officinale* at 10, 15, and 20 mg·mL^{-1}, with the highest concentration combined with DFO (100 μmol·L^{-1}) or Fer-1 (1 μmol·L^{-1}). SW480 cells were similarly treated at 5, 10, and 15 mg·mL^{-1}, with the highest dose combined with inhibitors. After 24 h, cells were fixed with 4% PFA, permeabilized with 0.1% Triton X-100, and blocked with 5% BSA. Primary antibody against GPX4 (1∶200) was applied overnight at 4 °C, followed by a fluorescent secondary antibody (1∶200) for 1 h. Nuclei were counterstained with DAPI for 15 min. Fluorescence signals were visualized using a confocal microscope (Leica, Germany).

2.13. Small interfering ribonucleic acid (siRNA) interference and plasmid transfection

siRNA constructs targeting GPX4 (siGPX4) and negative control siRNA (siCon) were synthesized by Suzhou Genepharma Co., Ltd. (Suzhou, China). The sense sequences were: siGPX4-1, 5′-CAGGGAGUAACGAAGAGAU-3′; siGPX4-2, 5′-GTGGATGAAGATCCAACCCAA-3′. The GPX4 overexpression plasmid (pcDNA3.1-GPX4) and empty vector control (pcDNA3.1) were obtained from Obio Technology (Shanghai) Corp., Ltd. Transfections were performed using Lipofectamine™ 3000 according to the manufacturer's protocol and maintained for 48 h. After transfection, HCT116 cells were treated with 20 mg·mL^{-1} *D. officinale*, and SW480 cells with 15 mg·mL^{-1} for 24 h. Post-treatment analyses included MTT assays, EdU detection, lipid peroxidation, MDA and GSH/GSSG measurements, and ΔΨm assessment, all conducted using established protocols.

2.14. Animal xenograft model

All animal procedures were conducted in accordance with institutional ethical guidelines approved by the Guangzhou University of Chinese Medicine Animal Ethics Committee (Approval No. 20220908, Guangzhou, China). Male BALB/c nude mice (4 weeks old; Certification No. 44007200125910) were obtained from Guangdong Medical Laboratory Animal Center (License SCXK 2018-0002) and housed under specific pathogen-free (SPF) conditions at the International Institute for Translational Chinese Medicine [SYXK(GZ)2024-0144], Guangzhou University of Chinese Medicine. HCT116 cells (2×10^6) were subcutaneously injected into the right axilla of each mouse. When tumor volume reached approximately 80 mm^3, mice were randomly assigned to six groups (n = 6 per group): (1) Model group (daily oral saline); (2) *D. officinale* low-dose group (1 g·kg^{-1}, orally daily); (3) medium-dose group (2 g·kg^{-1}, orally daily); (4) high-dose group (4 g·kg^{-1}, orally daily); (5) combination group (*D. officinale* 4 g·kg^{-1} daily orally plus Fer-1 5 mg·kg^{-1} every two days *via* intraperitoneal injection); (6) Oxa group (5 mg·kg^{-1} every two days *via* intraperitoneal injection). Tumor dimensions were measured daily with calipers, and volumes were calculated as (length × width^2)/2. On day 19, mice were euthanized, tumors were excised and weighed, and tissues were processed for histological (hematoxylin and eosin (H&E) staining), immunohistochemical (Ki67, GPX4), and biochemical analyses.

2.15. H&E staining

Tumor tissues were fixed in 10% neutral-buffered formalin, dehydrated through an ethanol gradient, and embedded in paraffin. Sections (4 μm thick) were mounted on glass slides, deparaffinized in xylene, and rehydrated in descending ethanol series. Staining was performed sequentially with Mayer's hematoxylin, differentiation in 1% acid ethanol, counterstaining with eosin Y, dehydration, and mounting with neutral balsam. Morphological features were evaluated using a microscope equipped with 20 × and 40 × objectives (Leica, Germany).

2.16. Immunohistochemistry (IHC)

Formalin-fixed, paraffin-embedded tissue sections (4 μm) underwent antigen retrieval in citrate buffer and endogenous peroxidase quenching. After washing with PBS-T, non-specific binding was blocked by incubation with 5% normal goat serum at room temperature. Sections were then incubated overnight at 4 °C with primary antibodies against GPX4 (1:200) and Ki67 (1∶150). After incubation with appropriate HRP-conjugated secondary antibodies, immunoreactivity was visualized using DAB as the chromogen, followed by counterstaining with hematoxylin. Images were acquired using a bright-field microscope (Leica, Germany) under standardized settings.

2.17. Statistical analysis

Data are expressed as mean ± standard deviation (SD). Group comparisons were performed using one-way ANOVA followed by Tukey's post hoc test (GraphPad Prism 9.0). A P value less than 0.05 was considered statistically significant.

3. Results

3.1. D. officinale suppresses CRC cell viability and proliferation in vitro

MTT assays demonstrated dose-dependent inhibition of CRC cell viability following 24-h exposure to *D. officinale*. Treatment with concentrations of 5–40 mg·mL^{-1} significantly reduced viability in HCT116 cells (Fig. 1A, $P < 0.001$) and SW480 cells (Fig. 1B,

$P < 0.05$ or $P < 0.001$). Oxa, used as a positive control, similarly suppressed viability in both cell lines (Figs. 1A and 1B, $P < 0.001$). Notably, *D. officinale* treatment (5–40 mg·mL^{-1}) induced minimal changes in the viability of non-cancerous NCM460 cells (Fig. 1C), indicating selective cytotoxicity toward cancer cells. Based on these results, subsequent experiments employed optimized concentrations: 10–20 mg·mL^{-1} for HCT116 and 5–15 mg·mL^{-1} for SW480.

Proliferation assays further confirmed the anti-CRC effects of *D. officinale*. Colony formation capacity was markedly impaired in treated cells (Figs. 1D and 1E, $P < 0.001$), with colony numbers inversely correlated to treatment dosage. EdU incorporation assays corroborated these findings, revealing dose-dependent reductions in DNA synthesis rates (Figs. 1F and 1G, $P < 0.05$ or $P < 0.001$). The proportion of EdU-positive cells decreased sharply, consistent with suppressed clonogenic potential.

3.2. *D. officinale* triggers ferroptosis in CRC cells

To evaluate the involvement of ferroptosis, MTT assays were performed in the presence of specific inhibitors, namely, deferoxamine (DFO) and Fer-1. Both agents significantly reversed the viability suppression induced by *D. officinale* in HCT116 and SW480 cells (Figs. 2A and 2B, $P < 0.01$ or $P < 0.001$). Similarly, supplementation with GSH reduced cytotoxicity (Figs. 2C and 2D, $P < 0.001$). Treatment with *D. officinale* increased MDA levels in CRC cells. This effect was attenuated by co-administration of DFO or Fer-1 (Figs. 2E and 2F, $P < 0.05$, $P < 0.01$, or $P < 0.001$). Conversely, the GSH/GSSG ratio was significantly reduced upon treatment but partially restored when inhibitors were co-administered (Figs. 2G and 2H, $P < 0.001$). Mitochondrial depolarization was observed via JC-1 staining, as indicated by an increased green/red fluorescence ratio in cells treated with *D. officinale*. This mitochondrial dysfunction was alleviated by ferroptosis inhibitors (Figs. 2I and 2J). C11-BODIPY assays demonstrated that lipid ROS accumulation induced by *D. officinale* was suppressed by DFO or Fer-1 (Figs. 3A–3D, $P < 0.01$ or $P < 0.001$). Intracellular Fe^{2+} levels were significantly elevated in treated cells (Figs. 3E and 3F), further confirming the activation of ferroptotic pathways.

3.3. *D. officinale* inhibits tumor growth *in vivo* via ferroptosis induction

A xenograft mouse model was utilized to assess the *in vivo* efficacy of *D. officinale* (Fig. 4A). No significant differences in body weight or organ indices were observed between treated and model groups, suggesting low systemic toxicity (Supplementary Fig. 2). Compared with the control group, both the *D. officinale* and Oxa treatment groups exhibited marked tumor suppression, as evidenced by reduced tumor volume (Figs. 4B–4D, $P < 0.05$ or $P < 0.001$) and tumor weight (Fig. 4E, $P < 0.05$ or $P < 0.01$). These

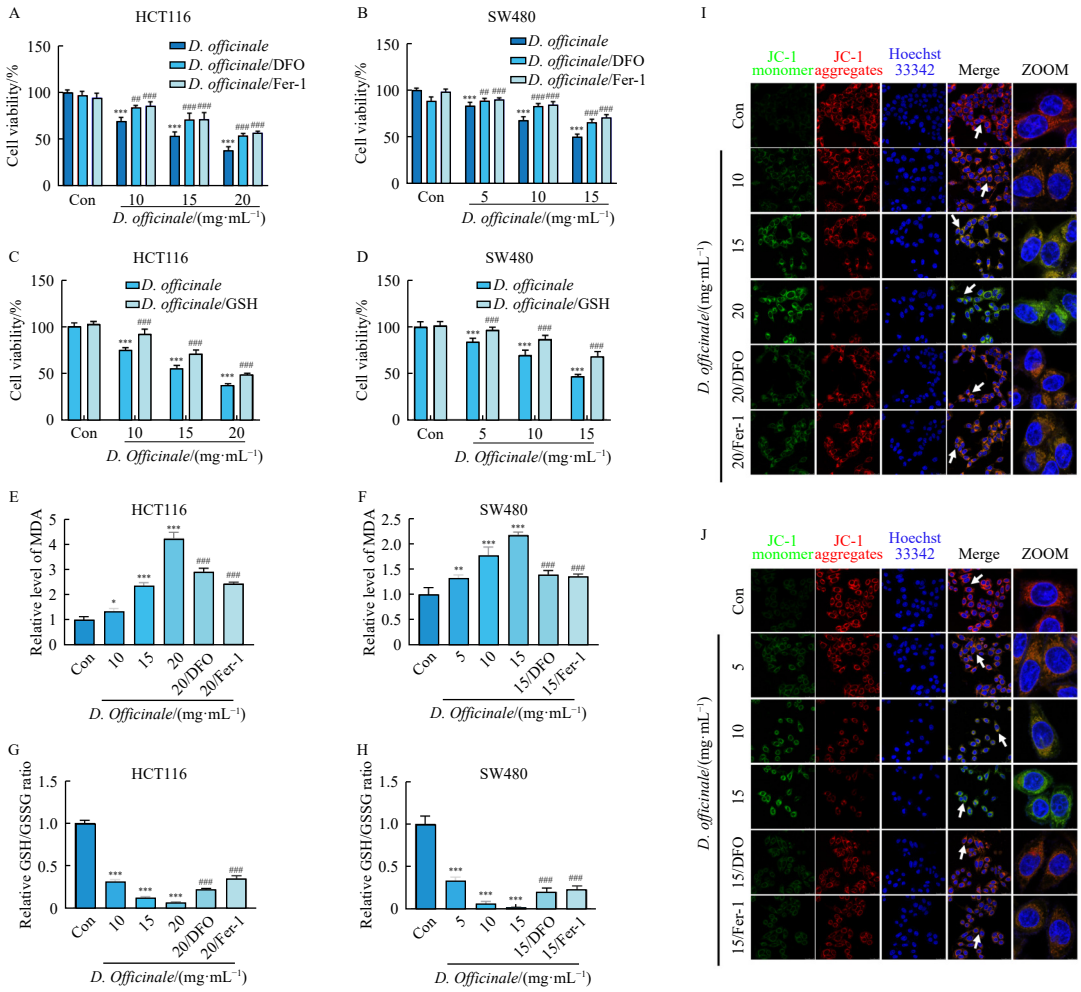

Fig. 2 *D. officinale* triggers ferroptosis in CRC cells. The viability of HCT116 (A) and SW480 (B) cells exposed to *D. officinale* was evaluated in the presence or absence of ferroptosis inhibitors (1 μmol·L^{-1} Fer-1 or 100 μmol·L^{-1} DFO) over a 24-h period. Cell viability following 24 h of *D. officinale* exposure was assessed both with and without GSH supplementation (C and D). Levels of MDA (panels E and F) and the GSH/GSSG ratio (G and H) were quantified in CRC cells after 24 h of *D. officinale* treatment, either alone or in combination with Fer-1 or DFO. The intracellular fluorescence of JC-1 monomers and aggregates in HCT116 (I) and SW480 (J) cells was monitored following 24 h of *D. officinale* treatment, with or without Fer-1 or DFO. Data are expressed as mean ± SD ($n = 3$). $^{*}P < 0.05$, $^{**}P < 0.01$, and $^{***}P < 0.001$ *vs* the control group; $^{\#\#\#}P < 0.001$ *vs* the *D. officinale*-treated group.

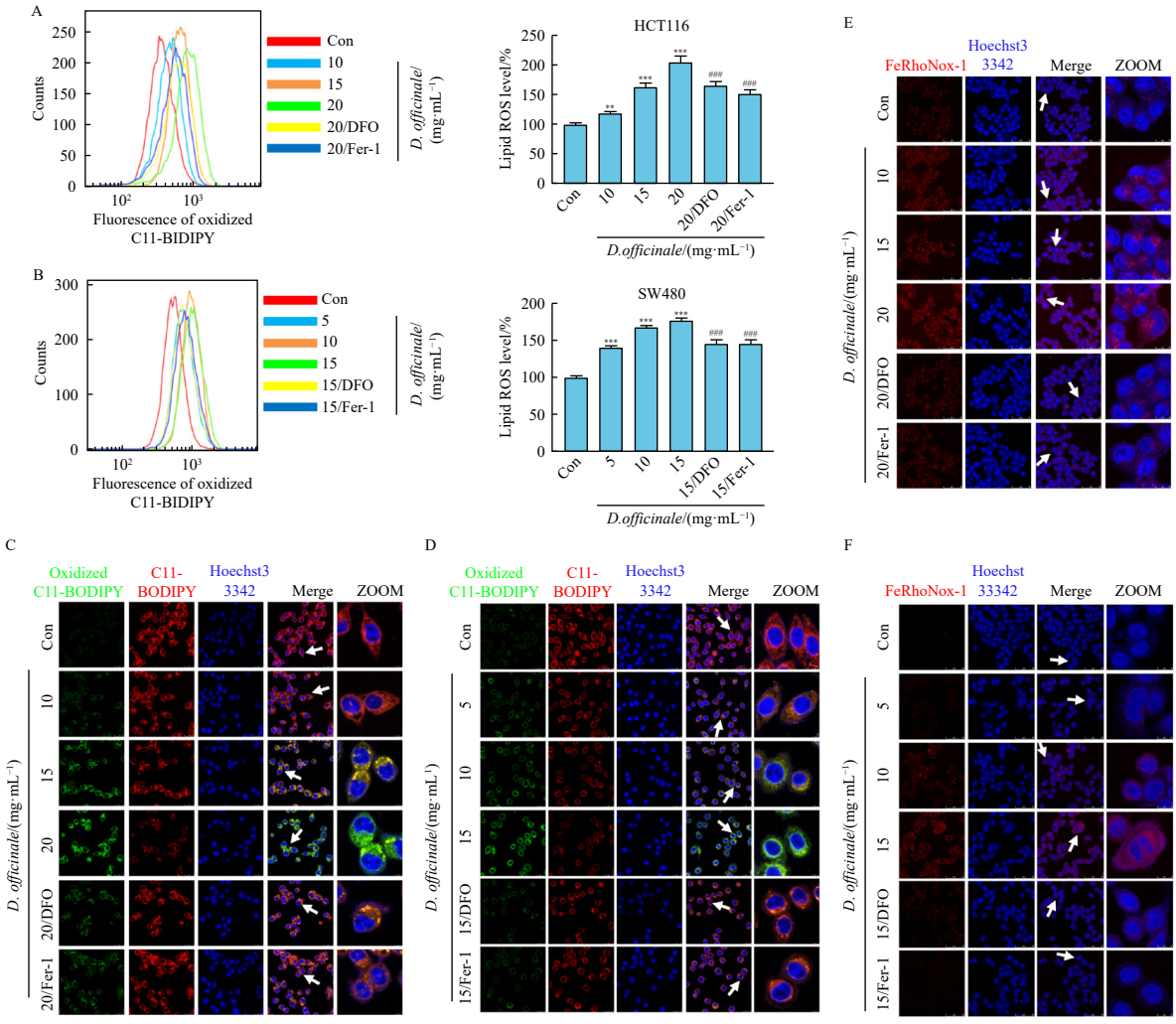

Fig. 3 *D. officinale* promotes lipid peroxidation and increases intracellular Fe^{2+} levels in CRC cells. After treating the cells with *D. officinale*, either alone or in combination with 1 μmol·L^{-1} Fer-1 or 100 μmol·L^{-1} DFO for 24 h, the intracellular fluorescence of C11-BODIPY and its oxidized form was analyzed using flow cytometry (A and B) and confocal microscopy (C and D). The intracellular Fe^{2+} concentrations were measured in HCT116 (E) and SW480 (F) cells following the same treatment conditions. Data are represented as mean ± SD (n = 3). $^{***}P < 0.001$ *vs* the control group; $^{###}P < 0.001$ *vs* the *D. officinale*-treated group.

anti-tumor effects were attenuated in the Fer-1 co-treatment group (Figs. 4B–4E, $P < 0.05$), indicating partial reversal of activity.

Histological analysis of H&E-stained tumors revealed diminished malignant proliferation in mice treated with *D. officinale* (Fig. 4F), an effect abrogated by Fer-1. Ki67 staining further demonstrated concentration-dependent reductions in proliferative activity following *D. officinale* treatment, while Fer-1 co-administration increased Ki67 positivity (Fig. 4G). Additionally, tumor tissues from *D. officinale*-treated mice exhibited elevated MDA levels (Fig. 4H, $P < 0.001$) and reduced GSH/GSSG ratios (Fig. 4I, $P < 0.001$), both of which were reversed by Fer-1. These

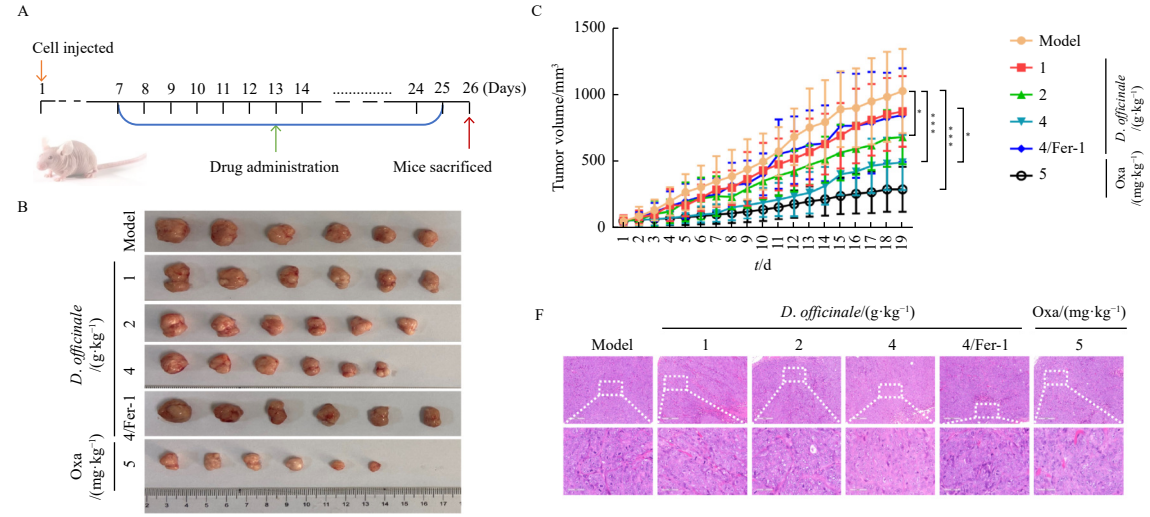

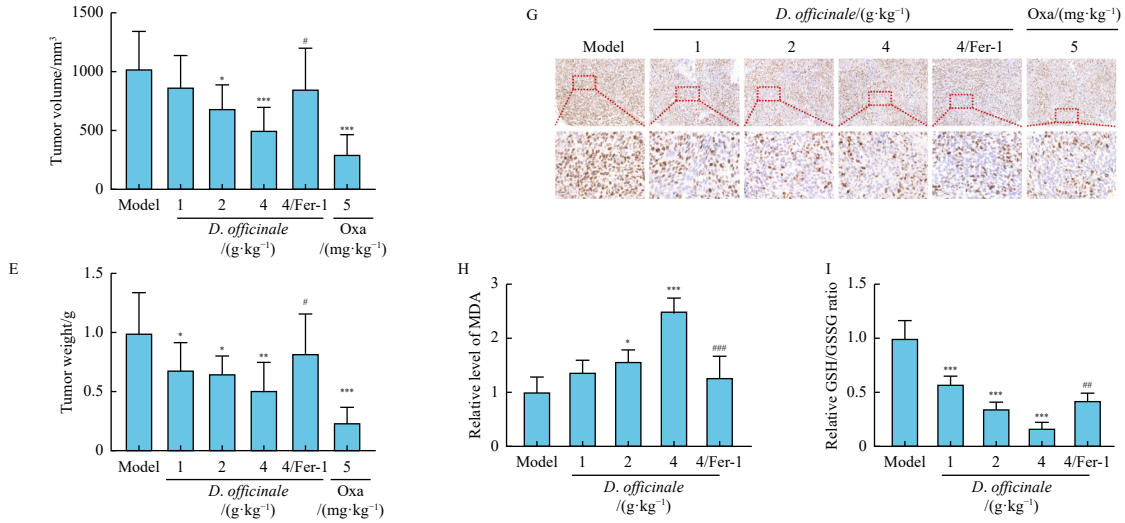

Fig. 4 *D. officinale* suppresses tumor growth *in vivo* through ferroptosis induction. The experimental design for the nude mouse xenograft tumor model (A). Visual representations of tumors from each group of mice (B). Tumor volumes (C and D) and tumor weights (E) were measured across groups. Representative images of H&E staining (F) and Ki67 immunohistochemistry (G) from xenograft tumors are presented for each group. The levels of MDA (H) and the GSH/GSSG ratio (I) were evaluated in colon tissues following *D. officinale* treatment. Data are expressed as mean ± SD (n = 6). $^{*}P < 0.05$, $^{**}P < 0.01$, and $^{***}P < 0.001$ *vs* the model group. $^{\#}P < 0.05$, $^{\#\#}P < 0.01$, and $^{\#\#\#}P < 0.001$ *vs* the *D. officinale* treated group.

findings confirm that ferroptosis plays a critical role in *D. officinale*-mediated tumor growth suppression *in vivo*.

3.4. *D. officinale* downregulates GPX4 expression

IHC and Western blot analyses demonstrated reduced GPX4 expression in *D. officinale*-treated CRC xenografts, which was restored upon co-administration of Fer-1 (Figs. 5A and 5B, $P < 0.05$ or $P < 0.001$). Western blot analyses further validated these results, showing marked decreases in GPX4 and SLC7A11 protein levels in treated CRC cells compared to controls (Figs. 5C and 5D, $P < 0.001$). To provide additional evidence, immunofluorescence staining was performed to assess GPX4 expression at the cellular level. The results confirmed diminished GPX4 expression in *D. officinale*-treated CRC cells *in vitro* (Figs. 5E and 5F, $P < 0.001$). Western blot analyses further showed that the downregulation of GPX4 by *D. officinale* was reversed by co-treatment with DFO and Fer-1 (Figs. 5G–5J, $P < 0.001$). These findings suggest that *D. officinale*-induced GPX4 downregulation is closely linked to ferroptotic mechanisms.

3.5. GPX4 mediates *D. officinale*-induced ferroptosis

To investigate the functional role of GPX4 in mediating *D. officinale*-induced ferroptosis, we established GPX4-overexpressing CRC cell lines (Supplementary Fig. 3). Our findings revealed that GPX4 overexpression markedly mitigated the suppressive effects of *D. officinale* on cell viability (Figs. 6A and 6B, $P < 0.001$) and proliferation (Figs. 6C and 6D, $P < 0.001$). Cells with elevated GPX4 expression maintained a higher GSH/GSSG ratio (Figs. 6E

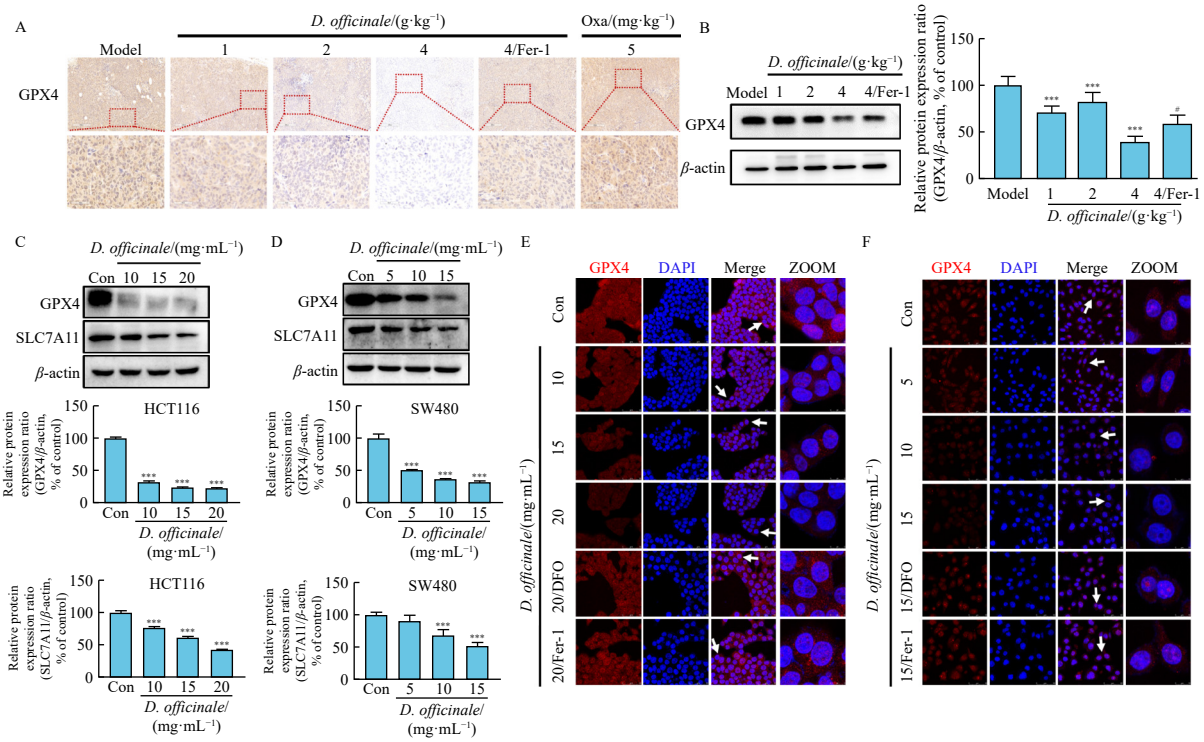

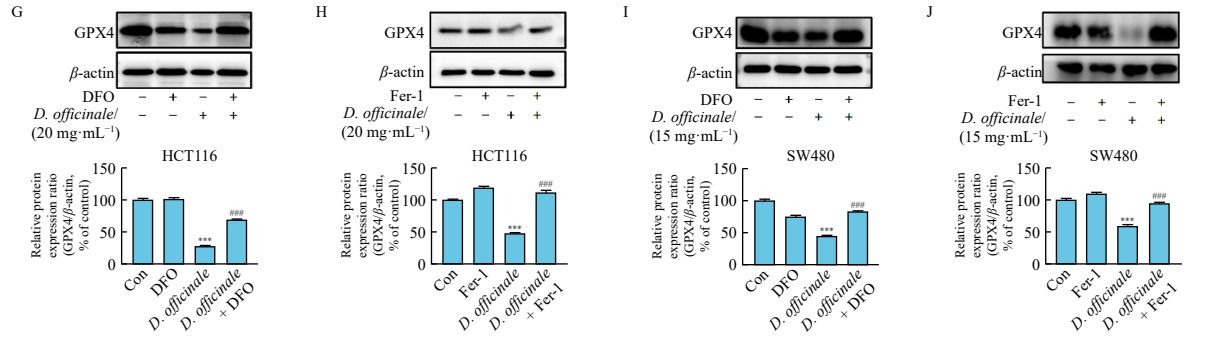

Fig. 5 *D. officinale* down-regulated the expression of GPX4 protein. The expression of GPX4 protein in colon tissues from each group of mice was evaluated using immunohistochemistry (A) and Western blot analysis (B) following treatment. In CRC cells, GPX4 protein levels were assessed *via* Western blot (C and D) and immunofluorescence (E and F) after treatment. The effect of *D. officinale* on GPX4 protein expression was examined in CRC cells both in the presence and absence of DFO (G and H) and Fer-1 (I and J). Data are presented as mean ± SD (n = 3). In panel B, $^{***}P < 0.001$ *vs* the model group, $^{\#}P < 0.05$ *vs* the *D. officinale* treatment group *in vivo*. In panels C–J, $^{***}P < 0.001$ *vs* the control group; $^{\#\#\#}P < 0.001$ *vs* the *D. officinale*-treated group *in vitro*.

and 6F, $P < 0.001$) and exhibited decreased MDA production (Figs. 6G and 6H, $P < 0.001$) upon *D. officinale* treatment. Moreover, GPX4 overexpression effectively counteracted the excessive lipid peroxidation triggered by *D. officinale* (Figs. 6I–6L, $P < 0.01$ or $P < 0.001$). Additionally, GPX4-overexpressing cells exhibited enhanced mitochondrial membrane potential (Δψm) following *D. officinale* exposure compared to wild-type cells (Figs. 6M and 6N).

To further validate the involvement of GPX4 in ferroptosis-mediated cell death, we generated GPX4-knockdown CRC models (Supplementary Fig. 3). The results indicated that GPX4 depletion significantly amplified the inhibitory impact of *D. officinale* on cell viability (Figs. 7A and 7B, $P < 0.001$) and proliferation (Figs. 7C and 7D, $P < 0.001$). Furthermore, *D. officinale* treatment

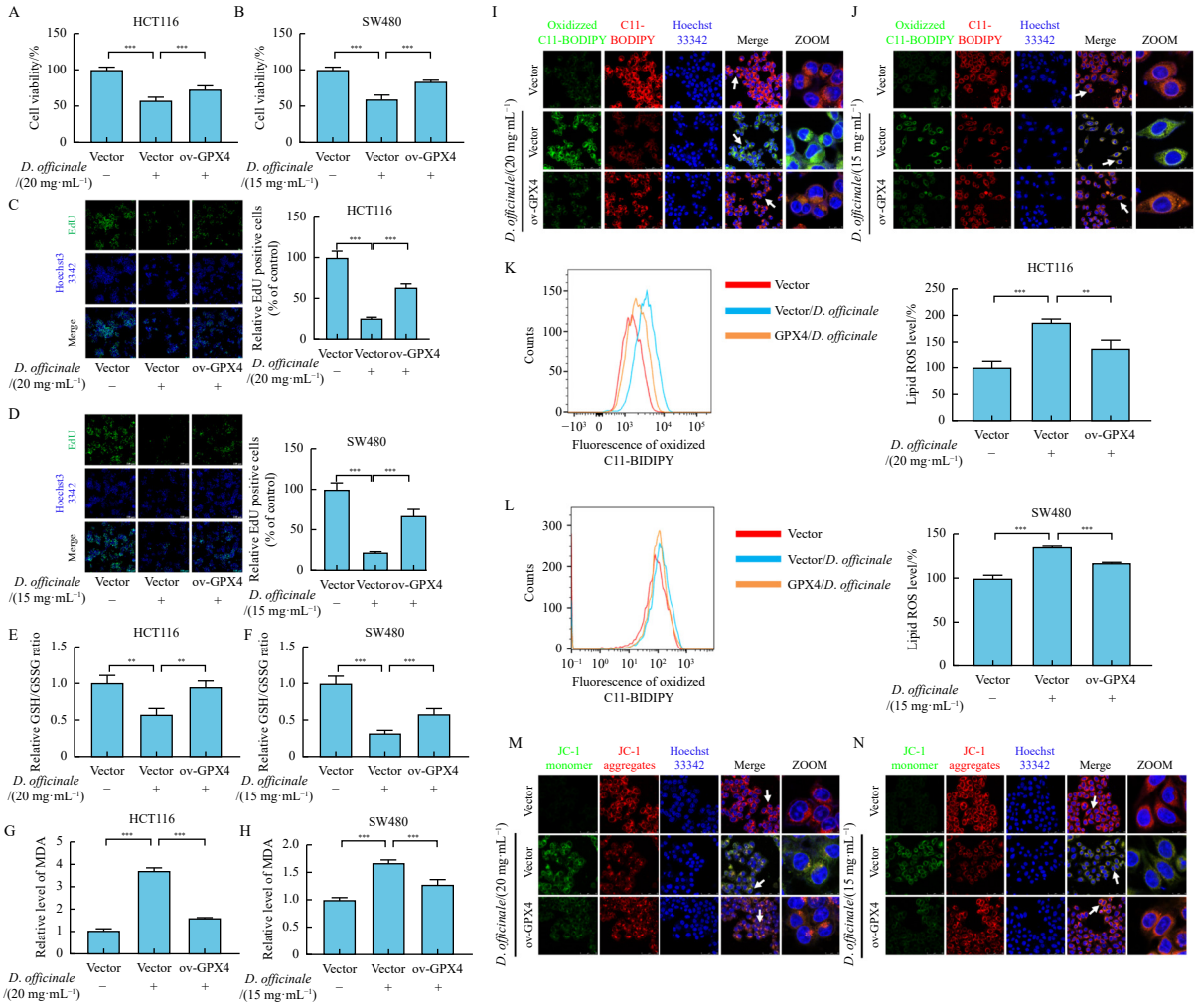

Fig. 6 Overexpression of GPX4 attenuates *D. officinale*-induced ferroptosis in CRC cells. Following *D. officinale* treatment, with or without GPX4 overexpression, cell viability was assessed using the MTT assay (A and B). Cell proliferation was evaluated through the EdU assay (C and D). The GSH/GSSG ratio (E and F) and MDA levels (G and H) were measured in CRC cells. Intracellular fluorescence of C11-BODIPY and its oxidized form was detected using confocal microscopy (I and J) and flow cytometry (K and L). Confocal microscopy was also employed to observe the intracellular fluorescence of JC-1 monomers and aggregates in CRC cells (M and N). Data are presented as mean ± SD (n = 3). $^{**}P < 0.01$ and $^{***}P < 0.001$ *vs* corresponding groups.

resulted in a more substantial reduction in the GSH/GSSG ratio (Figs. 7E and 7F, $P < 0.01$ or $P < 0.001$) and greater elevation of MDA levels (Figs. 7G and 7H, $P < 0.001$) in GPX4-depleted cells relative to wild-type cells. Additionally, GPX4 depletion markedly intensified *D. officinale*-induced lipid peroxidation (Figs. 7I–7L, $P < 0.01$ or $P < 0.001$) and led to a pronounced decline in Δψm in CRC cells exposed to *D. officinale* (Figs. 7M and 7N).

4. Discussion

CRC remains a significant global health burden, with rising incidence strongly associated with dietary habits and aging populations [22]. Although early detection through screening has improved survival outcomes, therapeutic options for advanced-stage CRC, particularly in cases involving chemoresistance and metastasis, remain limited, highlighting an urgent need for innovative treatment approaches [23]. This study provides robust evidence that *D. officinale* exerts anti-tumor effects against CRC by inducing ferroptosis, a regulated form of cell death driven by iron-dependent lipid peroxidation. Our results show that *D. officinale* downregulates GPX4, a key enzyme responsible for maintaining cellular redox homeostasis [7], thereby initiating a cascade of oxidative events culminating in mitochondrial dysfunction and cancer cell death. This mechanism aligns with emerging ferroptosis-targeted cancer therapies, yet distinguishes itself through the natural origin and multitargeted phytochemical profile of *D. officinale*, potentially offering advantages in safety and reduced risk of drug resistance compared to synthetic agents.

Ferroptosis has emerged as a promising selective anti-cancer strategy due to its dependence on iron metabolism and lipid peroxidation, processes frequently dysregulated in malignant cells [24]. Mechanistic analyses identify ferroptosis as the predominant mode of cell death, supported by three lines of experimental evidence: (1) characteristic biochemical markers, including elevated MDA levels, a collapsed GSH/GSSG ratio, and intracellular Fe^{2+} accumulation; (2) functional reversal by specific ferroptosis inhibitors, such as DFO and Fer-1; and (3) mitochondrial abnormalities, particularly depolarization of the mitochondrial membrane potential (Δψm), consistent with established ferroptotic morphology. GPX4, which relies on GSH to detoxify lipid hydroperoxides,

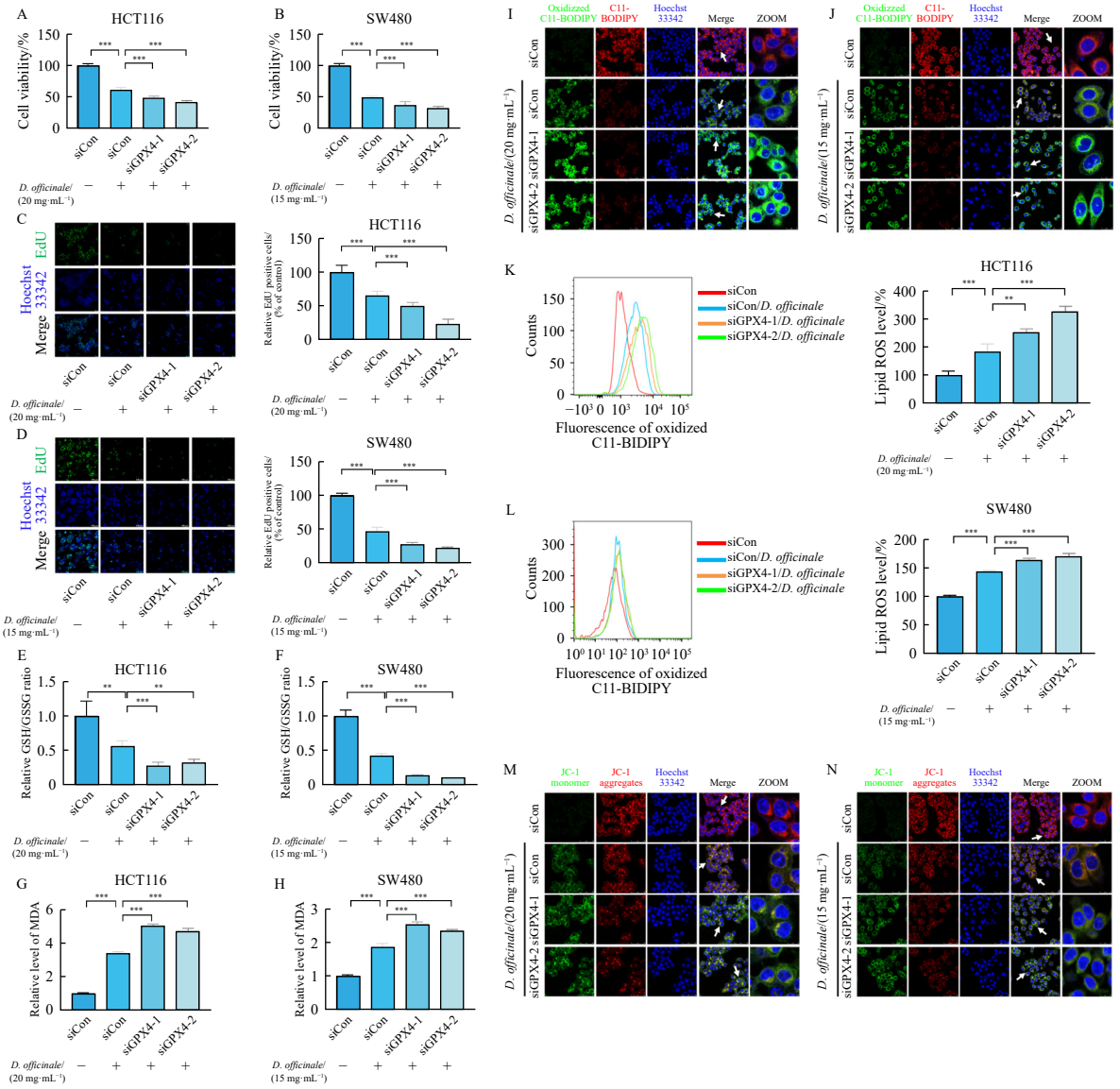

Fig. 7 GPX4 silencing exacerbates *D. officinale*-induced ferroptosis in CRC cells. Following *D. officinale* treatment, with or without GPX4 silencing, cell viability was assessed using the MTT assay (A and B). Cell proliferation was evaluated through the EdU assay (C and D). The GSH/GSSG ratio (E and F) and MDA levels (G and H) were measured in CRC cells. Intracellular fluorescence of C11-BODIPY and its oxidized form was detected using confocal microscopy (I and J) and flow cytometry (K and L). Confocal microscopy was also employed to observe the intracellular fluorescence of JC-1 monomers and aggregates in CRC cells (M and N). Data are presented as mean ± SD ($n = 3$). $^{**}P < 0.01$ and $^{***}P < 0.001$ *vs* corresponding groups.

acts as a central regulator in this pathway [25]. We demonstrate that *D. officinale* significantly reduces GPX4 expression both *in vitro* and *in vivo*, an effect that is reversed by Fer-1 and DFO. Genetic experiments further confirm the pivotal role of GPX4: overexpression rescues cell viability and suppresses lipid peroxidation, whereas silencing exacerbates ferroptotic cell death. These findings establish GPX4 as a critical mediator of *D. officinale*'s anticancer activity and highlight its potential as a molecular target for future therapeutic development.

Notably, mitochondrial depolarization and increased lipid ROS preceded overt cell death, suggesting that ferroptosis is directly initiated rather than occurring secondarily through necrosis [26]. This temporal sequence is consistent with recent models in which GPX4 inactivation triggers mitochondrial lipid peroxidation cascades [27]. However, the partial rescue observed with Fer-1 compared to DFO suggests that additional, iron-independent pathways may also contribute to the overall effect. This could involve modulation of other antioxidant systems by polysaccharide components of *D. officinale* [28]. Such a dual mechanism may enhance therapeutic efficacy while minimizing the likelihood of resistance development.

The selective toxicity of *D. officinale* toward CRC cells relative to NCM460 is particularly significant. This differential sensitivity likely stems from the heightened iron dependency and disrupted redox balance commonly found in cancer cells. Malignant cells typically exhibit increased iron uptake *via* transferrin receptors and diminished antioxidant capacity, rendering them more vulnerable to ferroptosis induction [17, 29]. In contrast, normal cells maintain tighter regulation of iron homeostasis and possess more robust antioxidant defenses, which may explain the relative sparing of NCM460 cells. This selectivity mirrors the therapeutic window targeted in conventional chemotherapy but is achieved here through a natural product, underscoring the potential of plant-derived compounds in precision oncology.

Comparative evaluation with synthetic ferroptosis inducers such as RSL3 and erastin reveals both similarities and distinctions [30, 31]. While these agents directly inhibit GPX4 or system x_c^- (a cystine/glutamate antiporter), their clinical application is hindered by off-target effects and suboptimal pharmacokinetics. In contrast, *D. officinale* likely acts through synergistic interactions among multiple bioactive constituents, including polysaccharides, flavonoids, and alkaloids, that collectively enhance efficacy and reduce the risk of resistance, a common limitation of monotherapies [8].

While this study establishes the GPX4-ferroptosis axis as central to *D. officinale*'s anti-tumor activity, several questions warrant further investigation. First, the specific bioactive constituents responsible for GPX4 suppression require isolation and characterization of their structure–activity relationships. Second, upstream regulators of GPX4 in *D. officinale*-treated cells should be elucidated using transcriptomic and proteomic profiling. Third, combination studies with standard-of-care therapies could explore synergistic effects and help define ferroptosis-related biomarkers for patient stratification. Finally, pharmacokinetic optimization through nano-formulation may overcome potential bioavailability limitations of *D. officinale*. Addressing these aspects could accelerate clinical translation and expand the role of *D. officinale* in modern oncology.

5. Conclusions

In conclusion, our study demonstrates that *D. officinale* significantly induces ferroptosis in CRC cells through downregulation of GPX4 expression (Fig. 8). These results establish *D. officinale* as a potent inducer of GPX4-mediated ferroptosis. This dual role not only supports its potential for clinical translation but also provides a robust experimental basis for developing novel anticolon cancer therapeutics.

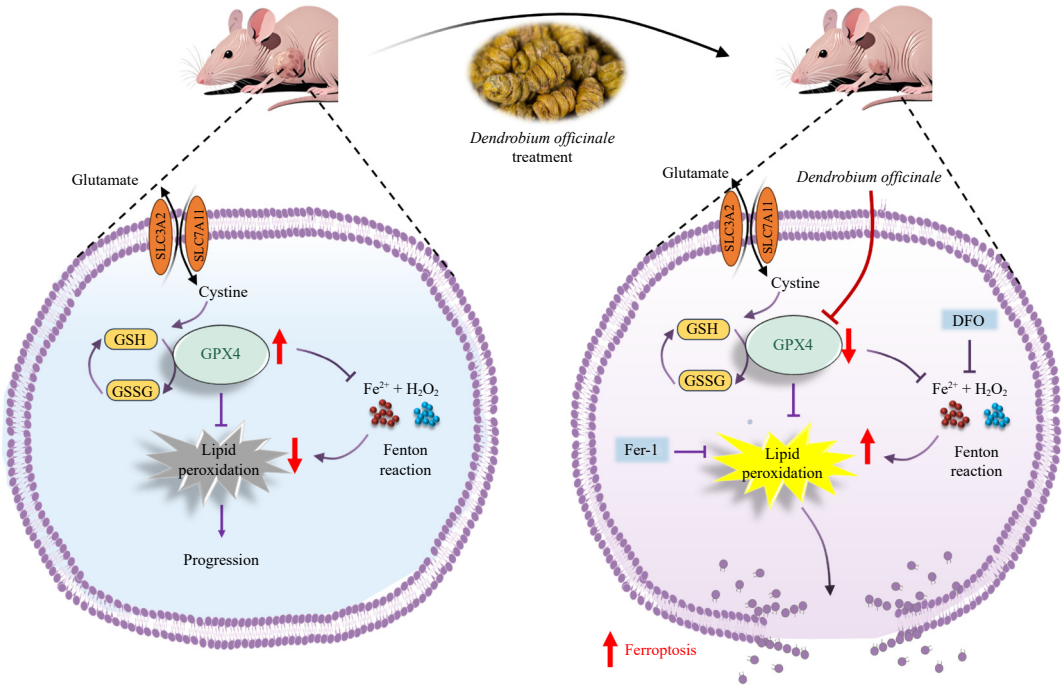

Fig. 8 Schematic representation of the proposed mechanism. *D. officinale* markedly induces ferroptosis in colon cancer cells by downregulating GPX4 expression. These findings suggest that *D. officinale* acts as a potent inducer of GPX4-mediated ferroptosis.

Funding

This work was supported by the Department of Education of Guangdong Province (No. 2023KTSCX024), the Project of Traditional Chinese Medicine Bureau of Guangdong Province (No.20251091), the Joint Funds of the National Natural Science Foundation of China (No. U22A20368), the Key-Area Research and Development Program of Guangdong Province (No.

2020B1111100004), Guangdong Basic and Applied Basic Research Foundation (No. 2020B1515130005), and Shenzhen Baoan District Science and Technology Innovation Bureau Project (Nos. 2022JD226 and 2023JD252).

Supporting information

Supplementary data associated with this article can berequested by sending E-mail to the corresponding authors.

Declaration of competing interest

These authors have no conflict of interest to declare.

References

1 Akiyama H, Zhao R, Ostermann LB, et al. Mitochondrial regulation of GPX4 inhibition-mediated ferroptosis in acute myeloid leukemia. *Leukemia*. 2024; 38(4):729-740. https://doi.org/10.1038/s41375-023-02117-2.

2 Cao W, Zhang X, Feng Y, et al. Lipid nanoparticular codelivery system for enhanced antitumor effects by ferroptosis-apoptosis synergistic with programmed cell death-ligand 1 downregulation. *ACS Nano*. 2024;18(26): 17267-17281. https://doi.org/10.1021/acsnano.4c04901.

3 Cheff DM, Huang C, Scholzen KC, et al. The ferroptosis inducing compounds RSL3 and ML162 are not direct inhibitors of GPX4 but of TXNRD1. *Redox Biol*. 2025;62:102703. https://doi.org/10.1016/j.redox.2023.102703.

4 Chen WH, Wu JJ, Li XF, et al. Isolation, structural properties, bioactivities of polysaccharides from *Dendrobium officinale* Kimura et. Migo: a review. *Int J Biol Macromol*. 2021;184:1000-1013. https://doi.org/10.1016/j.ijbiomac.2021.06.156.

5 Chu W, Wang P, Ma Z, et al. Ultrasonic treatment of *Dendrobium officinale* polysaccharide enhances antioxidant and anti-inflammatory activity in a mouse D-galactose-induced aging model. *Food Sci Nutr*. 2022;10(8):2620-2630. https://doi.org/10.1002/fsn3.2867.

6 Dekker E, Tanis PJ, Vleugels JLA, et al. Colorectal cancer. *Lancet*. 2019;394 (10207):1467-1480. https://doi.org/10.1016/s0140-6736(19)32319-0.

7 Hu JL, Wang W, Lan XL, et al. CAFs secreted exosomes promote metastasis and chemotherapy resistance by enhancing cell stemness and epithelial-mesenchymal transition in colorectal cancer. *Mol Cancer*. 2019;18(1):91. https://doi.org/10.1186/s12943-019-1019-x.

8 Jiang W, Tan J, Zhang J, et al. Polysaccharides from *Dendrobium officinale* improve obesity-induced insulin resistance through the gut microbiota and the SOCS3-mediated insulin receptor substrate-1 signaling pathway. *J Sci Food Agric*. 2024;104(6):3437-3447. https://doi.org/10.1002/jsfa.13229.

9 Jiang X, Stockwell BR, Conrad M. Ferroptosis: mechanisms, biology and role in disease. *Nat Rev Mol Cell Biol*. 2021;22(4):266-282. https://doi.org/10.1038/s41580-020-00324-8.

10 Li M, Yue H, Wang Y, et al. Intestinal microbes derived butyrate is related to the immunomodulatory activities of *Dendrobium officinale* polysaccharide. *Int J Biol Macromol*. 2020;149:717-723. https://doi.org/10.1016/j.ijbiomac.2020.01.305.

11 Liang J, Wu Y, Yuan H, et al. *Dendrobium officinale* polysaccharides attenuate learning and memory disabilities *via* anti-oxidant and anti-inflammatory actions. *Int J Biol Macromol*. 2019;126:414-426. https://doi.org/10.1016/j.ijbiomac.2018.12.230.

12 Lin A, Giuliano CJ, Palladino A, et al. Off-target toxicity is a common mechanism of action of cancer drugs undergoing clinical trials. *Sci Transl Med*. 2019;11(509):aaw8412. https://doi.org/10.1126/scitranslmed.aaw8412.

13 Lin Y, Zhang Y, Wang D, et al. Computer especially AI-assisted drug virtual screening and design in traditional Chinese medicine. *Phytomedicine*. 2022;107:154481. https://doi.org/10.1016/j.phymed.2022.154481.

14 Liu Y, Wan Y, Jiang Y, et al. GPX4: The hub of lipid oxidation, ferroptosis, disease and treatment. *Biochim Biophys Acta Rev Cancer*. 2023;1878(3): 188890. https://doi.org/10.1016/j.bbcan.2023.188890.

15 Niu B, Liao K, Zhou Y, et al. Application of glutathione depletion in cancer therapy: enhanced ROS-based therapy, ferroptosis, and chemotherapy. *Biomaterials*. 2021;277:121110. https://doi.org/10.1016/j.biomaterials.2021.121110.

16 Pan H, Gray R, Braybrooke J, et al. 20-Year risks of breast-cancer recurrence after stopping endocrine therapy at 5 years. *N Engl J Med*. 2017;377(19): 1836-1846. https://doi.org/10.1056/NEJMoa1701830.

17 Prutki M, Poljak-Blazi M, Jakopovic et al. Altered iron metabolism, transferrin receptor 1 and ferritin in patients with colon cancer. *Cancer Lett*. 2006;238(2):188-196. https://doi.org/10.1016/j.canlet.2005.07.001.

18 Ruan J, Zhang P, Zhang Q, et al. Colorectal cancer inhibitory properties of polysaccharides and their molecular mechanisms: a review. *Int J Biol Macromol*. 2023;238:124165. https://doi.org/10.1016/j.ijbiomac.2023.124165.

19 Yang J, Chen H, Nie Q, et al. *Dendrobium officinale* polysaccharide ameliorates the liver metabolism disorders of type II diabetic rats. *Int J Biol Macromol*. 2020;164:1939-1948. https://doi.org/10.1016/j.ijbiomac.2020.08.007.

20 Song X, Liu C, Zhang Y, et al. Sustainable extraction of ligustilide and ferulic acid from Angelicae Sinensis Radix, for antioxidant and anti-inflammatory activities. *Ultrason Sonochem*. 2023;94:106344. https://doi.org/10.1016/j.ultsonch.2023.106344.

21 Tang R, Xu J, Zhang B. et al. Ferroptosis, necroptosis, and pyroptosis in anticancer immunity. *J Hematol Oncol*. 2020;13(1):110. https://doi.org/10.1186/s13045-020-00946-7.

22 Ursini F, Maiorino M. Lipid peroxidation and ferroptosis: the role of GSH and GPx4. *Free Radic Biol Med*. 2020;152:175-185. https://doi.org/10.1016/j.freeradbiomed.2020.02.027.

23 Vasan N, Baselga J, Hyman D. A view on drug resistance in cancer. *Nature*. 2019;575(7782):299-309. https://doi.org/10.1038/s41586-019-1730-1.

24 Wang D, Liang W, Huo D, et al. SPY1 inhibits neuronal ferroptosis in amyotrophic lateral sclerosis by reducing lipid peroxidation through regulation of GCH1 and TFR1. *Cell Death Differ*. 2023;30(2):369-382. https://doi.org/10.1038/s41418-022-01089-7.

25 Wang K, Song M, Mu X, et al. Comparison and the lipid-lowering ability evaluation method discussion of *Dendrobium officinale* polysaccharides from different origins based on principal component analysis. *Int J Biol Macromol*. 2023;242(Pt 1):124707. https://doi.org/10.1016/j.ijbiomac.2023.124707.

26 Willems PH, Rossignol R, Dieteren CE, et al. Redox homeostasis and mitochondrial dynamics. *Cell Metab*. 2015;22(2):207-218. https://doi.org/10.1016/j.cmet.2015.06.006.

27 Xu X, Zhang C, Wang N, et al. Bioactivities and mechanism of actions of *Dendrobium officinale*: a comprehensive review. *Oxid Med Cell Longev*. 2022: 6293355. https://doi.org/10.1155/2022/6293355.

28 Xue D, Feng S, Zhao H, et al. The linkage maps of *Dendrobium* species based on RAPD and SRAP markers. *J Genet Genomics*. 2010;37(3):197-204. https://doi.org/10.1016/s1673-8527(09)60038-2.

29 Zhang K, Zhou X, Wang J, et al. *Dendrobium officinale* polysaccharide triggers mitochondrial disorder to induce colon cancer cell death *via* ROS-AMPK-autophagy pathway. *Carbohydr Polym*. 2021;264:118018. https://doi.org/10.1016/j.carbpol.2021.118018.

30 Zhang P, Zhang X, Zhu X, et al. Chemical constituents, bioactivities, and pharmacological mechanisms of *Dendrobium officinale*: a review of the past decade. *J Agric Food Chem*. 2023;71(41):14870-14889. https://doi.org/10.1021/acs.jafc.3c04154.